J Membrane Biol (2013) 246:821–831
DOI 10.1007/s00232-013-9552-9

Molecular Dynamic Simulation of Transmembrane Pore Growth

M. Deminsky · A. Eletskii · A. Kniznik · A. Odinokov · V. Pentkovskii · B. Potapkin

Received: 10 January 2013 / Accepted: 19 April 2013 / Published online: 10 May 2013

Abstract A molecular dynamic approach was applied for simulation of dynamics of pore formation and growth in a phospholipid bilayer in the presence of an external electric field. Processing the simulation results permitted recovery of the kinetic coefficients used in the Einstein–Smoluchowski equation describing the dynamics of pore evolution. Two different models of the bilayer membrane were considered: membrane consisting of POPC and POPE lipids. The simulations permitted us to find nonempirical values of the pore energy parameters, which are compared with empirical values. It was found that the parameters are sensitive to membrane type.

Keywords Molecular dynamic · Electroporation · Einstein–Smoluchowski equation

Introduction

The phenomenon of electroporation (EP) consists of the formation of pores in a cell membrane experienced by an electrical or electromagnetic field of various amplitude, duration, and frequency. The pore formation is accompanied by opening numerous water bridges in the membrane. With a hydrophilic water pathway across the hydrophobic interface, different water-soluble molecules can penetrate this barrier, which is totally prohibited otherwise.

Interest in this phenomenon is related to the possibility of permeation of various molecules and other biological objects such as genetic materials (Neumann et al. 1982; Mir et al. 1999; Suzuki et al. 1998), antigens (Neumann et al. 1999), viruses, and chemical reagents (Belehradek et al. 1993; Mir et al. 1995) through the membrane pores formed. This makes it possible to affect cell evolution (Weaver 2000), to affect its genetic nature (Mir et al. 1999), and, if necessary, to promote its killing (Neumann et al. 1999). Early experiments performed in the 1970s and 1980s (e.g., Kinosita and Tsong 1977; Neumann et al. 1982; Zimmermann et al. 1980; Zimmermann and Vienken 1982; Knight and Baker 1982) revealed that EP is not only an effective tool for inserting drugs inside a cell, but also a means for changing the genetic structure of the cell, which allows elimination of undesired hereditary defects in a living organism.

These studies were followed by the first experiments on inserting genes into animal cells (Neumann et al. 1982; Wong and Neumann 1982; Smithies et al. 1985; Potter 1988) and plant cells (Yang 1985; Fromm et al. 1986). Along with a change in the genetic nature of a cell, EP permits chemical reagents to act on tumor cells (Belehradek et al. 1993; Heller et al. 1998; Mir et al. 1998; Panje et al. 1998; Gehl and Geertsen 2000; Snoj et al. 2009), killing them. One can now speak of a new direction in chemotherapy: electrochemotherapy.

At present, directed EP-based methods have became widespread in clinical and academic practice. Commercial

M. Deminsky (✉) · A. Kniznik · B. Potapkin
Kintech Laboratory, Kurchatov Square 1, 123182 Moscow, Russia
e-mail: m.deminsky@hepti.kiae.ru; m.deminsky@kintechlab.com

M. Deminsky · A. Eletskii · A. Kniznik · B. Potapkin
State Research Center RF, Kurchatov Institute, Moscow, Russia

A. Odinokov
Photochemistry Center, Russian Academy of Sciences, Moscow, Russia

V. Pentkovskii
Moscow Institute of Physics and Technology, Dolgoprudny, Russia

devices providing a local action of DC or AC pulses of the electrical field of variable amplitude, duration, and frequency have been developed and tested (Marty et al. 2006). The parameters of the electric fields used vary within a wide range. The applied electric field strength varies from several kilovolts per centimeter up to several hundred kilovolts per centimeter, and pulse duration and frequency are changed from hundreds of femtoseconds to hundreds of milliseconds, and from kilohertz to dozens of kilohertz, respectively (Tekle et al. 2001; Deng et al. 2001; Pakhomov et al. 2007; Garner et al. 2007; Vernier et al. 2004, 2009; Buescher and Schoenbach 2003). Statistically valuable results of tests have been obtained that provide evidence of the effectiveness of EP in the treatment of some kinds of cancer tumors (Nuccitelli et al. 2006). It has been demonstrated that the overall effect of EP depends on pulse parameters (Canatella and Prausnitz 2001). The amplitude of the pulsed electric field promoting the EP is inversely proportional to the size of cell. The smaller the cell size, the higher is the necessary amplitude of the field (Gehl 2003). At the same time, the use of ultrashort pulses and high voltage results in organelle poration and a change in the permeabilization of the mammalian cell membrane (Pakhomov et al. 2007). Using 0.1–10 ms pulses with high field amplitude (kV/cm) provides the poration with effective transport through membrane, and cells remain viable (Chang 1989; Canatella and Prausnitz 2001). Enough long pulses (ms) at a low amplitude (fraction of kV) enhance the transport through membrane. The combination of short pulses of large amplitude with long pulses of low amplitude permits high permeability and effective transport of molecules such as DNA (Rabussay and Widera 2002).

The further development of EP-based approaches to the operation of a living cell calls for a deeper understanding of the key attendant processes. Standard methods of experimental investigation of these processes (see, e.g., Hibino et al. 1991; Tekle et al. 1994; Gabriel and Teissié 1997; Huang et al. 2003) do not sufficiently provide such an understanding because both physical characteristics and the time evolution of pores cannot be determined with sufficient accuracy. Therefore, many details of the EP mechanism remain unclear, thus creating a demand for the development of theoretical models.

The main problem arising in the theoretical description of pore evolution in the presence of an external electrical field relates to an evaluation of the time-dependent pore size distribution function (PSDF). The main approach to this problem is based on the solution of the Einstein–Smoluchowski equation for PSDF. Pore evolution proceeds as a stochastic process that may be described through a few energy parameters (Pastushenko et al. 1979; Abidor et al. 1979). These parameters are usually chosen empirically by fitting calculated results and experimental data. Such an approach promotes an understanding the physical mechanisms responsible for the interaction between the electrical field and the cell membrane. However, the experimental data can only be compared with the results of a sophisticated multistep calculation procedure, which involves many fitting parameters.

Several recent publications, however, have been devoted to molecular dynamic (MD) simulations of the EP process (Tieleman et al. 2003; Tarek 2005; Hu et al. 2005; Boeckmann et al. 2008; Vernier et al. 2009; Levine and Vernier 2010; Sun et al. 2011), describing at the molecular level the pore creation process and their subsequent evolution. Disadvantages of the MD approach relate to a rather high computing time cost and a sensitivity of calculation of results to the form of the intermolecular interaction potential and to the number of particles involved in the simulation model. Therefore, despite the importance of the EP problem for medicine and physiology—as well as the numerous practical advances in the use of EP in medicine and gene engineering—the interconnections between parameters of the electrical field applied to a cell of a specific nature and the time evolution of the size of membrane pores remain empirical. This hampers an understanding the mechanisms of interaction of the electrical field with lipid structures and hinders the further development of EP-based methods of cell control. The absence of a comprehensive theory of EP is caused by the extraordinarily sophisticated and not yet fully established structure of cell membranes. Lipid molecules incorporated into the cell membranes present macromolecular compounds that consist of many thousands of atoms, with adducts of various charges and orientations. Direct simulation of such structures (Tarek 2005; Breton et al. 2012) results in insuperable calculation difficulties, which are compounded by uncertainties in the parameters of lipid molecules (Dickey and Faller 2008).

In order to overcome the above-mentioned disadvantages of the existing approaches to describing the electrical field-induced pore evolution, we propose to combine them. Here we use the MD simulation for evaluation, in a non-empirical way, of the key parameters used in the stochastic model for the description of PSDF evolution. First we determine the principal parameters that determine pore evolution within the framework of the stochastic process and effective potential. Then the atomic description of a pore is clarified and details of the MD simulation are addressed. Next, the ways to extract the data of interest from the MD trajectory are elaborated and the results of the implementation of these algorithms are provided. Finally, we discuss the obtained results.

The pore evolution

The process of pore creation and growth is essentially stochastic. The time evolution of the PSDF $n(r,t)$ is usually represented as a diffusion process in some potential, which can be expressed through the Einstein–Smoluchowski equation (Abidor et al. 1979; Pathria 1972):

$$\frac{\partial n(r,t)}{\partial t} = \frac{D}{k_B T}\frac{\partial}{\partial r}\left[n(r,t)\frac{\partial W(r)}{\partial r}\right] + D\left[\frac{\partial^2 n(r,t)}{\partial r^2}\right] + S(r), \quad (1)$$

where r is the radius of a pore, D is the diffusion coefficient, and k_B and T represent the Boltzmann constant and temperature, respectively. The overall process is governed by two functions: the energy of the hydrophilic pore $W(r)$ and the pore creation rate $S(r)$. The hydrophilic potential $W(r)$ can be attributed to the energy difference between the membrane with a pore and the membrane without any defects in it. This potential is usually expressed as (Abidor et al. 1979; Weaver and Mintzer 1981; Neu and Krassowska 1999)

$$W(r) = 2\pi\gamma r - \pi\sigma r^2 + \left(\frac{C}{r}\right)^4 - \pi a_p V^2 r^2. \quad (2)$$

Here γ refers to the edge energy of the pore, σ is the energy per unit area for intact membrane, a_p is the capacitance per unit area of the pore, V represents the transmembrane potential, and the term controlled by parameter C is responsible for the repulsion between lipid heads covering the pore interior. The characteristic behavior of the hydrophilic potential (Eq. (2)) is presented in Fig. 1 for various values of the transmembrane potential, with typical values of the potential parameters from the works of Freeman et al. (1994) and Sugar (1979): $\gamma = 1.8 * 10^{-11}$ J/m; $\sigma = 10^{-3}$ J/m^2; $C = 9.7 * 10^{-15}$ J$^{1/4}$m; $a_p = 0.069$ F/m^2. The dash-dotted line in Fig. 1 indicates the potential of the hydrophobic pore (Isambert 1998). The processes of pore formation and evolution under the electric field go from the changing of the inner structure from hydrophilic to hydrophobic type (see the crossing of lines 1 and 2 in Fig. 1) and further growth in the potential, which depends on the value of the applied transmembrane potential (Fig. 1, lines 1–3). The presence of the local minimum (about 1 nm), where the intermediate state of the pore can be stabilized, also depends on the absolute value of V.

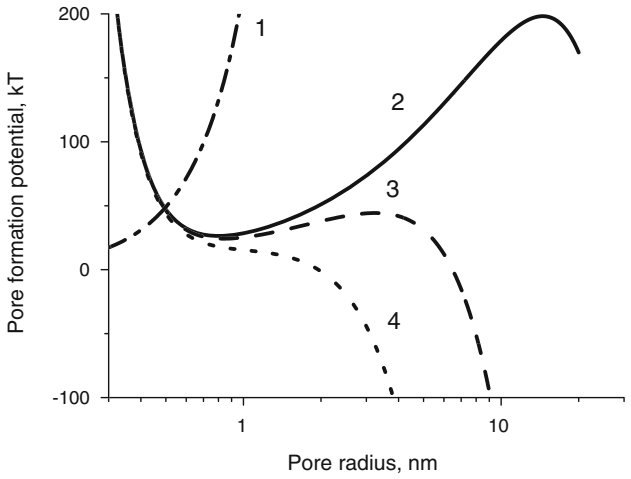

Fig. 1 Hydrophobic (*1*) and hydrophilic pore potentials for three different voltages applied to the membrane: (*2*) 0 V, (*3*) 0.25 V and (*4*) 0.5 V

The total effect is controlled by the rate of pore growth and the rate of pore creation. The latter represents a process of sharp electrical breakdown of the intact lipid membrane. Details of this process at the molecular level are still not well established. In past several decades, the event of pore birth was accounted for as a purely stochastic motion of the lipid molecules constituting the membrane. However, more recent studies that invoke MD simulations indicate that the process of pore creation is composed of a number of successive steps of different nature (Levine and Vernier 2010). We do not deal with the phenomenon of pore creation in the present study. Instead, we focus on the growth of a pore after it has appeared, so the last term in Eq. (1) will be omitted henceforth. Our main goal is to determine the functional form of $W(r)$ and the value of the diffusion coefficient D. Such numerical estimates seem to be novel and provide new reasoning for the existing model ideas in the theoretical description of EP.

Methods

Definition of the Model

In order to describe the pore growth via the MD simulation in terms of the continuous dielectric theory, one needs to establish the interconnection between the continuous geometrical objects and discrete particle distribution. We use the following approach. The lipid bilayer of phosphatidylcholine (POPC) and phosphatidylethanolamine (POPE) is regarded as a model of the membrane (Hu et al. 2005). The boundary between the lipid bilayer and the surrounding water is defined through the position of some representative point in the lipid head group. The position of the phosphorus atom will be used further at this point (Levine and Vernier 2010). Although these atoms undergo strong thermal fluctuations, the average boundary surface can be plotted (Fig. 2). This surface specifies two parallel planes as a border of the flat membrane and some region of space

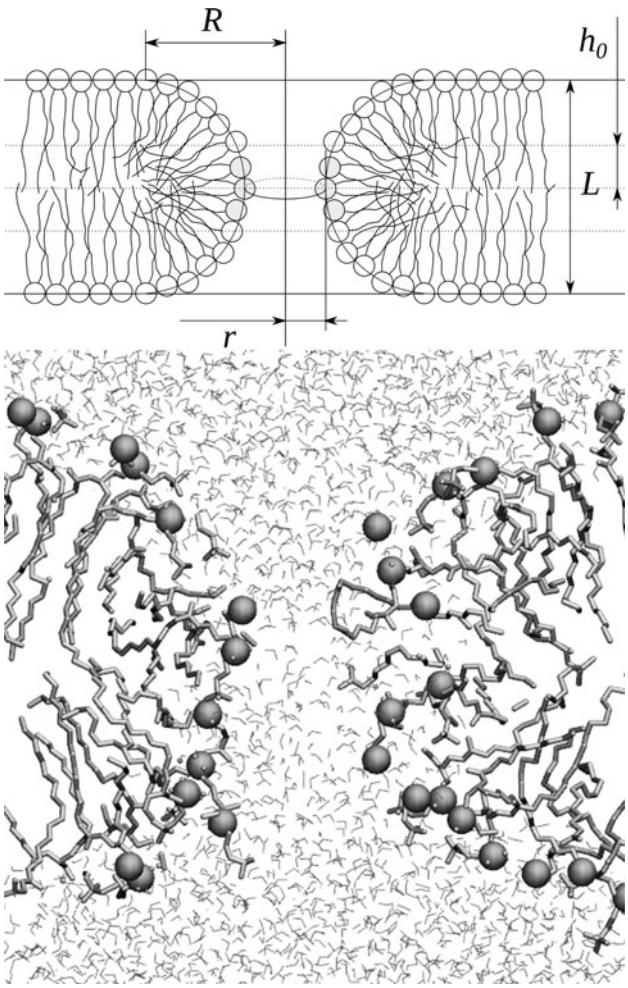

Fig. 2 Cross section of a transmembrane pore and definition of the underlying geometrical parameters. Schematic representation (*top*) and snapshot from an MD simulation (*bottom*) for the POPC bilayer

that is contained between these planes as an inner volume of the pore. Strictly speaking, a pore has an irregular shape, although for rough consideration it can be represented as an object with an axial symmetry. The cross-sectional diameter of a pore is not constant, which can be easily seen in Fig. 2.

In the following text, we will take the quantity r as an estimate for the pore radius (Fig. 2). The r represents the radius of the complex pore shape in the middle of the bilayer, i.e., in the narrowest place. To compute the instantaneous value of r from the position of all atoms at the given MD trajectory step, one needs to sample all the phosphorus atoms located in the limit of the predefined distance h_0 from the middle of the membrane (filled with gray in Fig. 2). The projection of these points on the x–y plane, which is parallel to the bilayer, forms an irregularly shaped circle. Then this projection is approximated by a circle via the least squares method. The value of r is defined as the radius of this circle.

It should be noted that the pore radius defined as described above may not be equal to that in the continuous model. The first physical reason is that the quantity r in Fig. 2 corresponds to the most narrow place, so the effective radius can be larger. The second reason is that the construction of the dividing surface in Fig. 2 is based on an arbitrarily chosen atom type (phosphorus). If another choice is made (e.g., nitrogen), the radius can differ. To treat these ambiguities, we propose to regard the effective pore radius $\tilde{r}$ (used in the continuous model) as $\tilde{r} = r + \delta$, where δ is a constant correction. Within such an approach, all derivatives with respect to r remain the same, but only the radius itself is indefinite. To obtain its precise value, some considerations beyond the current simulation must be provided. Or if the desired result is not very sensitive to r, all calculations can be done without any correction, as the value of δ is expected to be not very large compared to the radius.

Simulation Details

All the MD simulations were performed by Gromacs software, version 4.5.4 (van der Spoel et al. 2010). OPLS (optimized potentials for lipid simulations) force field–united atom parameters modified by Berger et al. (1997) were used for lipid molecules, while the simple point charge model (Berendsen et al. 1981) was used for water. The initial structure and topology files for the POPC bilayer were borrowed from Peter Tieleman of the University of Calgary (http://moose.bio.ucalgary.ca).

The system consisted of 128 POPC molecules arranged in the bilayer orthogonal to the z axis. The total number of water molecules was 6,606 ($\sim$50 molecules per lipid). The calculations involved four steps. In the beginning, the system was equilibrated for about 1 ns. At that stage, an average area per lipid was 0.68 nm^2, which slightly exceeded the measured value 0.65 nm^2 (Lantzsch et al. 1994). After that, an external electrostatic field of magnitude 0.3–0.5 V/nm was applied, so the pore creation process was observed during about next 3 ns. The direction of the electric field coincided with the membrane-surface normal z. The calculation time of pore formation was determined by two factors: the narrowest radius of the pore in the membrane layer plane should be larger then that of quasi-equilibrium state; and the largest distance between lipid head group from opposite sites of the formed pore is significantly less than the simulation slab scale of 6–9 nm. After its completion, on the third stage, the field was turned off, and the pore started to shrink. The characteristic timescale of the radius decay was about 300 ps, so after 2 ns of simulation, the pore seemed to reach its equilibrium state of minimum radius (this state corresponds to the local minimum of the function $W(r)$ in Fig. 1). A decision about

reaching the quasi-equilibrium state was taken from an analysis of the variation of the pore radius vs. time, in accordance with the procedure described above. Ten initial configurations were extracted from this 2 ns trajectory where the system is in a state of quasi-equilibrium. As the last step, the configurations of the system obtained were used as the initial state for the MD simulations.

Lipid bilayer and surrounding water were separately coupled with a velocity rescaling thermostat (Bussi et al. 2007) having a reference temperature of 310 K and a relaxation time of 0.2 ps. The system was also coupled with a semi-isotropic weak coupling barostat (Berendsen et al. 1984) at 1 atm with a relaxation time of 2 ps and isothermal compressibility of 4.5×10^{-5} bar^{-1} in the x–y plane and 0 bar^{-1} along the z axis (Hu et al. 2005). All the short-range interactions were cut off at 1.2 nm. The long-range part of the electrostatic interactions was calculated by the particle-mesh Ewald algorithm (Darden et al. 1993). Bond lengths were constrained using the SETTLE algorithm (Miyamoto and Kollman 1992) for water molecules and LINCS algorithm (Hess et al. 1997) for lipids. Each simulation run produced a 2 ns trajectory. The time step of MD simulations was 2 fs, the list of nearest neighbors was updated every ten steps, and the positions of all atoms in the system were stored every 50 steps.

Calculations of the pore radius were performed with the aid of the specially created VMD (Humphrey et al. 1996) script. The distance parameter $h_0 = 20$ Å was used.

Calculations were performed on the Kurchatov Institute cluster HPC1 (http://computing.kiae.ru/resources/hpc1), which consisted of 336 nodes of an Intel Xeon (2.33 GHz). Every MD trajectory was calculated using 48 nodes for a characteristic time of 1–5 ns that demanded about 2–10 h of calculation time at an average performance of 55 gigaflops. Time accounting shows that the main resources were spent for the neighbor search procedure and for calculation of the force in the framework of the particle-mesh Ewald method.

Estimation of the Pore Potential via the MD Simulation

Drift of a Brownian Particle in an External Potential

Suppose we have an ensemble of particles that can diffuse in the potential $W(r)$. If at time $t = 0$ all the particles are at the same point r_0, then their distribution function has the form $n(r, t = 0) = \delta(r - r_0)$ and its time evolution can be expressed as (Gardiner 2004)

$$n(r,t) = \frac{1}{\sqrt{2\pi D t}} \exp\left[-\frac{(r - r_0 - vt)^2}{2Dt}\right], \tag{3}$$

where

$$v = -\frac{D}{k_B T} \nabla W(r). \tag{4}$$

Equation (3) describes the motion of mean value r with velocity v, along with the diffusion process in the shifted coordinate $r' = r - vt$. This behavior is valid when the radius dependence of $\nabla W(r)$ is negligible.

Multiplying both sides of the Eq. (1) by r and integrating from 0 to infinity, we obtain

$$\frac{\partial \langle r \rangle}{\partial t} = -\frac{D}{k_B T} \langle \nabla W(r) \rangle, \tag{5}$$

where $\langle \cdots \rangle$ denotes the averaging over r. When the distribution function has the form of a single sharp peak and $W(r)$ can be regarded as a linear function within this peak, we can replace the averaged quantities in Eq. (5) by their local counterparts, e.g., taken from the point of the maximum of $n(r,t)$.

When the magnitude of the electric field applied to the lipid membrane is large enough, the local maximum of the function $W(r)$ vanishes (Fig. 1), so all the pores located at $r_{\min}$ increase their size monotonically (disregarding diffusion behavior at small distances). Given a set of MD trajectories describing such a process, one can evaluate the function $\langle r(t) \rangle$. Although this function has a linear form, expression (3) holds, and the value of the diffusion coefficient can be derived from the time dependence of the radius mean square displacement:

$$\left\langle (r - vt)^2 \right\rangle = Dt. \tag{6}$$

Then the gradient of the pore energy potential $W(r)$ can easily be obtained from Eq. (5).

Diffusion as a Random Walk Process

The time dependence of the pore radius is an essentially continuous function. But if regarded as an array of values taken at a discrete set of time moments t_i (which is always the case in the MD simulation), the function $r(t_i)$ represents a realization of the random walk process. If the time interval between two subsequent steps Δt is large enough, then this process is also Markovian. The most general way to describe the Markovian process in terms of the distribution function is by the Fokker–Planck equation (Gardiner 2004):

$$\frac{\partial n(r,t)}{\partial t} = -\frac{\partial}{\partial r}[K_1(r,t) n(r,t)] + \frac{\partial^2}{\partial r^2}[K_2(r,t) n(r,t)]. \tag{7}$$

This expression reduces to Eq. (1) if the drift parameter $K_1(r,t)$ and diffusion parameter $K_2(r,t)$ are defined as

$$K_1(r,t) = \frac{D}{k_B T} \nabla W(r),\ K_2(r,t) \equiv D.$$

These quantities relate to the first and second moments of the distribution function:

$$K_1(r,t) = \frac{1}{\Delta t}\int_0^\infty (r'-r)p(r',\, t+\Delta t|r,\, t)\mathrm{d}r', \tag{8}$$

$$K_2(r,t) = \frac{1}{\Delta t}\int_0^\infty (r'-r)^2 p(r',\, t+\Delta t|r,\, t)\mathrm{d}r'. \tag{9}$$

These integrals can be calculated numerically by dividing the r axis into the bins and subsequently collecting the indices of starting bins and magnitudes for all jumps (events of radius change). The values of functions $K_1(r)$ and $K_2(r)$ in the bin i are equal, correspondingly, to the mean value and mean square value of the radius change for all the jumps starting from this bin, divided by the time step. The functions $K_1(r)$ and $K_2(r)$ are supposed to be time independent, which is always the case for diffusion processes without explicit time dependence of the potential.

Parameters of the Pore Energy Function

In the absence of the external electric field, the system exists near the minimum of the $W(r)$. In this region, the second term of Eq. (2) is at least in 20 times less than the other two ($\sigma = 10^{-3}$ J/m^2, Freeman et al. 1994), so this expression can be written as

$$W(r) = 2\pi\gamma r + \left(\frac{C}{r}\right)^4. \tag{10}$$

If we denote

$$\omega = \frac{\mathrm{d}^2 W(r_{\min})}{\mathrm{d}r^2},$$

we can express the remaining parameters of $W(r)$ as follows:

$$\gamma = \frac{1}{10\pi}\omega r_{\min}, \tag{11}$$

$$C = \sqrt[4]{\frac{\omega}{20}}(r_{\min})^{\frac{3}{2}}. \tag{12}$$

The values of ω and $r_{\min}$ can be obtained from the MD simulation through the calculation of the moments of the distribution function (see Eqs. (8) and (9)). For example, the behavior of the first moment $K_1(r)$ near the minimum of $W(r)$ determines both values of $r_{\min}$ and of $[d^2W(r_{\min})]/dr^2$, in the absence of the electric field, while the mean square displacement of the pore radius gives an effective diffusion coefficient D in case of a high value of the electric field of $2\pi\gamma \ll a_p V^2 r$. Whether found parameters of the pore potential $W(r)$ are local or whether their values can be safely extrapolated to the region of larger radii will be discussed below.

Results

Calculations with Finite Field Intensities

A set of MD trajectories was obtained for the applied electrical field strengths of 0.3 and 0.5 V/nm (Fig. 3). The corresponding $r(t)$ curves are arranged in the narrow beam around their average value $\langle r(t)\rangle$. It can be easily seen that $\langle r(t)\rangle$ has a linear region at short times. This fact allows the use of Eqs. (3)–(6) within this time interval. It can be also noted that for sufficiently high transmembrane potential V, the functional form $W(r)$ implies an accelerated pore growth. However, the computed value $\langle r(t)\rangle$ has a linear time dependence at the initial interval and decelerates after that. At long times, the pore radius approaches its asymptotic value, which is about half of the box side ($\sim$30 Å). This effect is the essential consequence of the limited box size used in the simulations. It is significant to note that this limitation does not affect the calculation because the diffusion coefficient is determined by the mean square displacement of pore radius at the initial stage of pore evolution near $r_{\min}$.

The mean square displacement of all the MD trajectories from their average value is shown in Fig. 4. During the first 100–150 ps, the calculated points coincide well with the linear trend for both field intensities. In this region, the model of a Brownian particle drifting in the linear external potential is physically meaningful, and Eq. (6) provides a simple way to determine the value of the diffusion

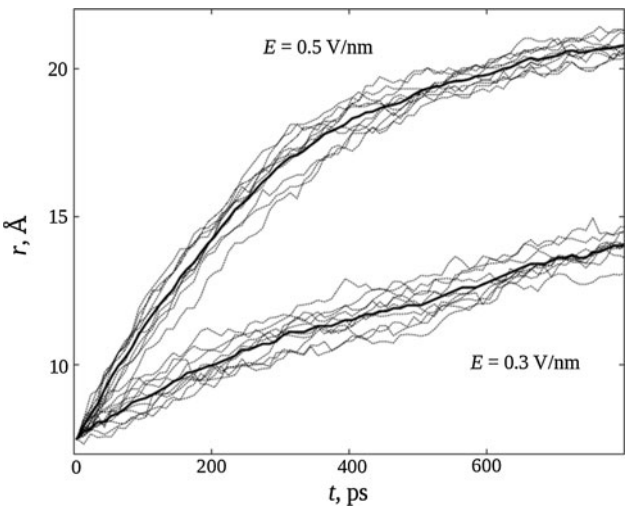

Fig. 3 Time evolution of the pore radii. The *thick line* represents the average value; the results for ten independent MD trajectories are shown by *dotted curves*

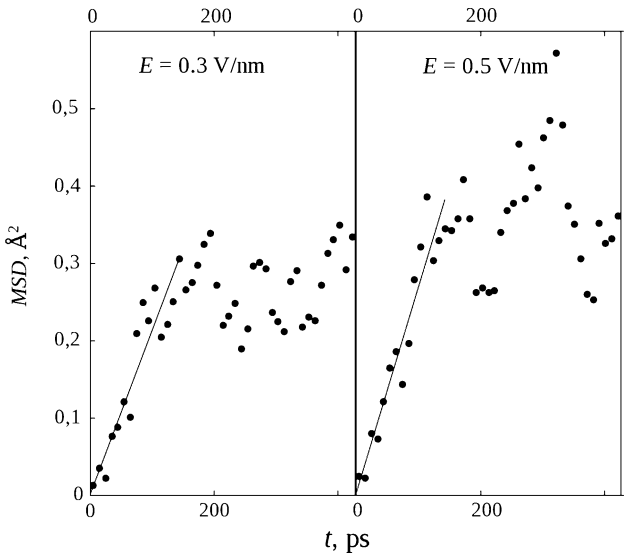

Fig. 4 Mean square displacement of the pore radius as a function of time (see Eq. (6))

coefficient. From the slope of the line in Fig. 4, one can find $D = (2.1 \pm 0.1) \times 10^{-11}\,\mathrm{m}^2/\mathrm{s}$ for the case of $E = 0.3$ V/nm and $D = (2.6 \pm 0.1) \times 10^{-11}\,\mathrm{m}^2/\mathrm{s}$ for the case of $E = 0.5$ V/nm.

Thermal Fluctuations

The above-described algorithm of the pore radius calculation implies that the obtained value is a linear function of the coordinates of the phosphorus atoms in chosen lipid molecules. It is thus subjected to permanent thermal fluctuations, which are inevitable for the motion of these molecules. Thermal motions in the system are represented by the vibrations of the atoms around their current equilibrium positions. Such motions appear as a high-frequency addition to the diffusion process, which in turn is dictated by the random displacement of the centers of equilibrium occurring at a larger timescale.

Thermal fluctuations distort the Markovian behavior of the function $r(t)$ at short times, so they must be eliminated in order to obtain parameters for the diffusion process. One way to do this is to smooth the curve $r(t)$ over some core. If m is the number of the points in the given core, then the smoothed function $r^{sm}(t)$ is defined as

$$r^{sm}(t_j) = \frac{1}{m}\sum_{i=1}^{m} r(t_j)$$

Thus the total number of points in the array $r^{sm}(t_j)$ is m times lesser than that in the original array $r(t_i)$. The result of such a procedure is shown in Fig. 5, where the core size is expressed in terms of the corresponding time interval. Although the sampling is not good enough to produce

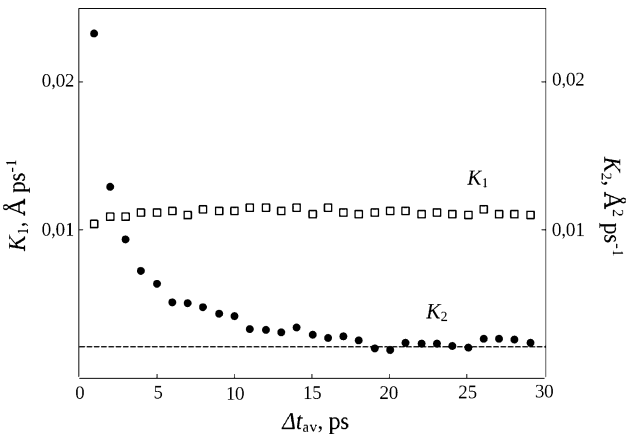

Fig. 5 Dependences of the Fokker–Planck parameters K_1 and K_2 of the time interval used to average the initial data obtained from the MD simulations. The *dotted line* represents an asymptotic value of K_2 determined from Eq. (6). The external electric field is 0.3 V/nm

reliable curves $K_1(r)$ and $K_2(r)$, the radius-independent values K_1 and K_2 have been obtained by averaging over the initial linear interval 0–120 ps. The shift parameter K_1 is almost independent of the core size, as there is no preferred direction for thermal fluctuations. Conversely, the mean square displacement K_2 is strongly affected by this effect and reaches its asymptotic value only for a smoothing core of 10 ps and more.

Calculations with Zero Field Intensity

The shape of the radial dependence of the pore energy $W(r)$ near the minimum can be extracted from the simulation without external field (see Eqs. (11) and (12)). The

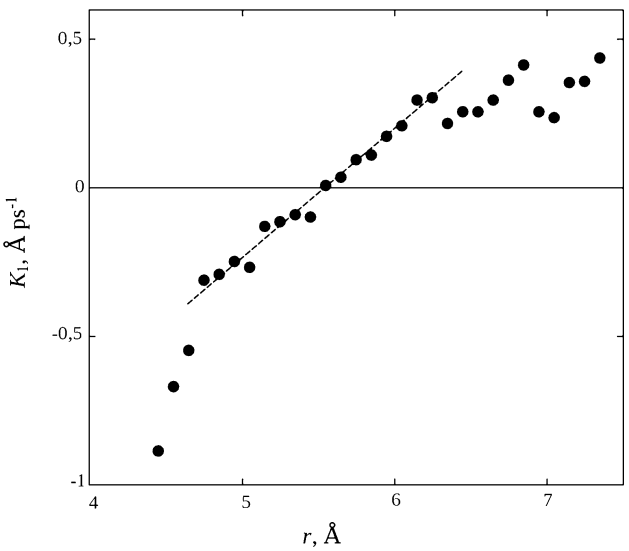

Fig. 6 Drift parameter K_1 as a function of radius. A point of the intersection of the curve with the x-axis defines $r_{\min}$, the minimum point of the potential $W(r)$

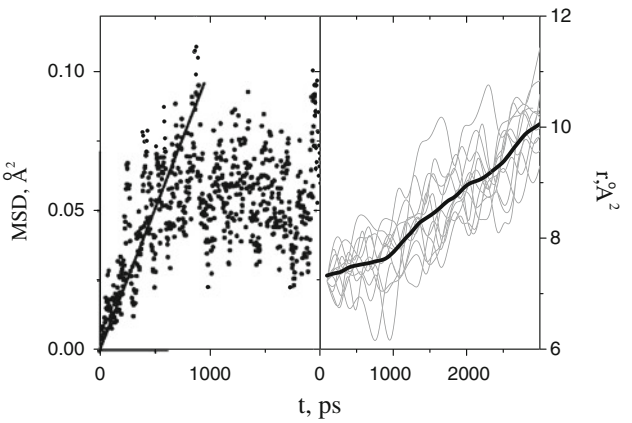

Fig. 7 Mean square displacement (*left*) and time evolution (*right*) of the pore radii for the POPE bilayer at an electric field of 0.3 V/nm

behavior of $K_1(r)$ is shown in Fig. 6. The point $r_{\min}$ corresponds to the zero value of the function $\nabla W(r)$ and consequently $K_1(r)$. The pore radius distribution function has a peak near the minimum of $W(r)$, so the sampling needed for the calculation of integral (8) provides quite smooth curve. At the larger distances, vast fluctuations occur. Moreover, the central curve perfectly fits a linear approximation (shown by a dotted line in Fig. 6) and serves as a solid basis for determination of the second derivative of $W(r)$.

The above-mentioned effect of thermal fluctuations hinders the determination of the diffusion coefficient. It can be easily seen from the fact that the mean square displacement within minimal smoothing core duration of 10 ps is comparable with the total width of the equilibrium distribution, so the value of K_2 after the smoothing procedure is strongly affected by the limited width of the potential well. $K_1(r)$ does not suffer from thermal fluctuations, and the curve in Fig. 6 can be easily plotted. The slope of this curve determines the second derivative of the function $K_1(r)$ near the minimum. Previous calculations for nonzero external field provide the value of the diffusion coefficient, so the shift coefficient is determined by $W(r)$. Then the parameters of this function are extracted via Eqs. (11) and (12). The obtained values are shown in Table 1, along with the diffusion coefficient.

Sensitivity to the Type of Bilayer and the Force Field Model

In order to estimate the sensitivity of obtained results to the type of the membrane, similar calculations were performed for the POPE bilayer. Initial structure and topology were taken as in the case of POPC from the source (http://moose.bio.ucalgary.ca). This system consisted of 340 molecules and 6,729 water molecules forming a bilayer. The simple point charge model was used for water. Other calculation parameters and the methodology used were similar to those described above for POPC bilayer calculations. The equilibrated configuration of the system was subjected to the external uniform electric field. In contrast to POPC results, it was found that poration does not occur when the initial value of the electric field is below 0.5 V/nm. The pore formation takes place for a characteristic time—about 4 ns at an electric field of 1 V/nm. Evolution of the pore nucleus was investigated after equilibration of the pore formed. Equilibration time was 2 ns. Investigation of the pore growth was further carried out at an electric field of 0.3 V/nm. Evolution of the pore radii is shown on the right side of Fig. 7. Comparison of the calculations for POPE and POPC bilayers shows that the rate of the radii growth in the first case is much smaller than in the second one. For example, the initial rate of the pore radii growth is 13 and 1 Å/ns for POPC and POPE bilayers, respectively. The possible reasons why this is so are discussed next; it is probably concerned with the difference in structure of the POPC and POPE membranes.

The mean square displacement of MD trajectories (15 trajectories for POPE bilayer) from their average value is shown on the left side of Fig. 7. A linear time dependence is observed for the initial 500–700 ps, which can be treated as particle drifting. In this case, the effective diffusion coefficient can easily be determined from the slope, which results in $D = (8.5 \pm 0.2) \times 10^{-13}\,\mathrm{m}^2/\mathrm{s}$. This value is

Table 1 Parameters of the poration model: calculated values and previous estimates

Parameter	Symbolic name	Calculated value	Model estimate	References
Diffusion coefficient (m^2/s)	D	2.5×10^{-11} POPC, 8.5×10^{-13} POPE	5×10^{-14}	Freeman et al. (1994)
Edge energy of a pore (J/m)	γ	1.3×10^{-9}	1.8×10^{-11}	Freeman et al. (1994) and Glaser et al. (1988)
Constant in a repulsive term ($J^{1/4}$ m)	C	2.4×10^{-14}	9.7×10^{-15}	Neu and Krassowska (1999)

POPC phosphatidylcholine, *POPE* phosphatidylethanolamine

about 30 times less than that for the POPC bilayer (Table 1).

Discussion

MD simulation of the time evolution of a lipid membrane experienced by the electrical field permits us to evaluate the pore parameters engaged in the Einstein–Smoluchowski Eq. (1). The quantities γ and C determined on the basis of such a calculation are more or less reasonable in comparison with those found in an empirical manner by fitting the solution of the Einstein–Smoluchowski Eq. (1) with experimental data on the field-induced permeability of cell membranes.

The value of the diffusion coefficient D calculated in our work differs considerably from that accepted by earlier authors. However, the calculations for POPE bilayer demonstrate an approach of the effective diffusion coefficient to the empirical value. Such a feature can be reasoned by a sensitivity of the calculation results to the type of the lipids and the details of the interaction potential between the neighboring lipids. Indeed, the POPE bilayer has a more compact structure in comparison with POPC. The average surface per lipid group in the POPE bilayer is about 51 Å^2, while that for POPC is about 68 Å^2. It leads to a more intensive interaction of lipid groups in the first type of the bilayer and it leads to a reduction of the effective diffusion coefficient in the Einstein–Smoluchowski equation. For example, if we suppose that the dipole–dipole interaction provides the stabilization of the external layer and limits the rate of the system reconstruction at pore growth, it is possible to roughly estimate the effect of the interaction on the diffusion coefficient through Eq. (9):

$$\frac{D_{\text{POPE}}}{D_{\text{POPC}}} = \frac{K_2^{\text{POPE}}}{K_2^{\text{POPC}}} \sim \exp\left(\frac{W_{\text{POPC}} - W_{\text{POPE}}}{kT}\right) \sim \frac{1}{60}, \qquad (13)$$

where W_{POPC} and W_{POPE} are the dipole–dipole interaction energies for POPC and POPE bilayers, respectively. If we take the characteristic value of the dipole moment of the lipid head group to be 19 D (Bechinger and Seelig 1991) and the average value of the distribution of the tilt angles of the dipoles to be 59° (Siu et al. 2008), the ratio of the diffusion coefficient is about 1/60, which is in a rough agreement with the ratio obtained in the MD experiments.

Let us note that the empirical estimations for all three parameters obtained in our calculations were originally derived from the numerical experiments for a standard membrane (Barnett and Weaver 1991). In these experiments, although a qualitative match was achieved, the output characteristics differed by experiment by several times. Another reason for discrepancy in C and γ values is that these constants are slightly dependent on the pore radius definition, so a direct comparison is actually hindered. Many other factors exist that can affect the calculation results. For example, a real cell membrane that experiences an external electrical field can behave differently than the lipid bilayer modeled in this work. Indeed, the real membrane does not have a plane shape but rather a curved shape, and pores form at surface sites containing transmembrane proteins or lipid domain boundaries (Antonov et al. 1980). Moreover, a real membrane is immersed in salt (ionic solution), which may also change the characteristics of the membrane. Applied MD experiments are closely related to electric field experiments with high voltage and short pulses. However, it is unclear how the results of such experiments can be extended to low-voltage experiments where charge imbalance is responsible for EP phenomena (Kramar et al. 2012).

Acknowledgments Supported in part by Grant of Government of Russian Federation in accordance with government regulation N220 (09.04.210).

References

Abidor IG, Arakelyan VB, Chernomordik LV, Chizmadzhev YA, Pastushenko VF, Tarasevich MR (1979) Electric breakdown of bilayer membranes: 1. The main experimental facts and their qualitative discussion. Bioelectrochem Bioenerg 6:37

Antonov V, Petrov W, Molnar A, Predvoditelev D, Ivanov A (1980) Appearance of single-ion channels in unmodified lipid bilayer-membranes at the phase transition temperature. Nature 283:585

Barnett A, Weaver J (1991) Electroporation: a unified, quantitative theory of reversible electrical breakdown, and rupture. Bioelectrochem Bioenerg 25:163

Bechinger B, Seelig J (1991) Interaction of the electric dipoles with phosholipid head groups. Biochemistry 30:3923–3929

Belehradek M, Domenge C, Luboinski B, Orlowski S, Belehradek JJ, Mir LM (1993) Electrochemotherapy, a new antitumor treatment. First clinical phase III trial. Cancer 72:3694

Berendsen HJC, Postma JPM, van Gunsteren WF, Hermans J (1981) Interaction models for water in relation to protein hydration. In: B. Pullman (ed) Intermolecular forces. Reidel, Dordrecht

Berendsen HJC, Postma JPM, van Gunsteren WF, DiNola A, Haak JR (1984) Molecular dynamics with coupling to an external bath. J Chem Phys 81:3684–3690

Berger O, Edholm O, Jähnig F (1997) Molecular dynamics simulations of a fluid bilayer of dipalmitoylphosphatidylcholine at full hydration, constant pressure, and constant temperature. Biophys J 72:2002–2013

Boeckmann RA, de Groot BL, Kakorin S, Neumann E, Grubmueller H (2008) Kinetics, statistics, and energetics of lipid membrane electroporation studied by molecular dynamics simulations. Biophys J 95:1837

Breton M, Delemotte L, Silve S, Mir L, Tarek M (2012) Transport of siRNA through lipid membranes driven by nanosecond electric pulses: an experimental and computational study. J Am Chem Soc 134:13938

Buescher ES, Schoenbach KH (2003) Effects of submicrosecond, high intensity pulsed electric fields on living cells-intracellular electromanipulation. IEEE Trans Dielect Electr Insul 10:788

Bussi G, Donadio D, Parrinello M (2007) Canonical sampling through velocity rescaling. J Chem Phys 126(014):101

Canatella PJ, Prausnitz M (2001) Prediction and optimization of gene transfection and drug delivery by electroporation. Gene Ther 8:1464

Chang D (1989) Cell poration and cell fusion using an oscilating electric field. Biophys J 56:641

Darden T, York D, Pedersen L (1993) Particle mesh Ewald: an n•log(n) method for Ewald sums in large systems. J Chem Phys 98:10089–10092

Deng J, Schoenbach KH, Buescher ES, Hair PS, Fox PM, Beebe SJ (2001) The effects of intense submicrosecond electrical pulses on cells. Biophys J 84:2709

Dickey A, Faller R (2008) Examining the contributions of lipid shape and headgroup charge on bilayer behavior. Biophys J 95:2636

Freeman SA, Wang MA, Weaver JC (1994) Theory of electroporation of planar bilayer membranes: predictions of the aqueous area, change in capacitance, and pore–pore separation. Biophys J 67:42–56

Fromm ML, Taylor P, Walbot V (1986) Stable transformation of maize after gene transfer by electroporation. Nature 319:791

Gabriel B, Teissié J (1997) Direct observation in the millisecond time range of fluorescent molecule asymmetrical interaction with the electropermeabilized cell membrane. Biophys J 73:2630

Gardiner CW (2004) Handbook of stochastic methods, 3rd edn. Springer, New York

Garner AL, Chen G, Chen N, Sridhara V, Kolb JF, Swanson RJ, Beebe SJ, Joshi RP, Schoenbach KH (2007) Ultrashort electric pulse induced changes in cellular dielectric properties. Biochem Biophys Res Comm 362:139

Gehl J (2003) Electroporation: theory and methods, perspectives for drug delivery, gene therapy and research. Acta Physiol Scand 177:437

Gehl J, Geertsen P (2000) Efficient palliation of hemorrhaging malignant melanoma skin metastases by electrochemotherapy. Melanoma Res 10:585

Glaser RW, Leikin SL, Chernomordik LV, Pastushenko VF, Sokirko AI (1988) Reversible electrical breakdown of lipid bilayers: formation and evolution of pores. Biochim Biophys Acta 940:275–287

Heller R, Jaroszeski MJ, Reintgen DS, Puleo CA, DeConti RC, Gilbert RA, Glass LF (1998) Treatment of cutaneous and subcutaneous tumors with electrochemotherapy using intralesional bleomycin. Cancer 83:148

Hess B, Bekker H, Berendsen HJC, Fraaije JGEM (1997) LINCS: a linear constraint solver for molecular simulations. J Comput Chem 18:1463–1472

Hibino M, Shigemori M, Itoh H, Nagayama K, Kinosita K (1991) Membrane conductance of an electroporated cell analyzed by submicrosecond imaging of transmembrane potential. Biophys J 59:209

Hu Q, Viswanadham S, Joshi RP, Schoenbach KH, Beebe SJ, Blackmore PF (2005) Simulations of transient membrane behavior in cells subjected to a high-intensity ultrashort electric pulse. Phys Rev E 71(031):914

Huang Y, Sekhon NS, Borninski J, Chen N, Rubinsky B (2003) Instantaneous, quantitative single-cell viability assessment by electrical evaluation of cell membrane integrity with microfabricated devices. Sens Actuator 105:31

Humphrey W, Dalke A, Schulten K (1996) VMD—visual molecular dynamics. J Mol Graph 14:33–38

Isambert H (1998) Understanding the electroporation of cells and artificial bilayer membranes. Phys Rev Lett 80:3404

Kinosita K, Tsong TY (1977) Formation and resealing of pores of controlled sizes in human erythrocyte membrane. Nature 268:438

Knight DE, Baker PF (1982) Calcium-dependence of catecholamine release from bovine adrenal medullary cells after exposure to intense electric fields. J Membr Biol 68:107

Kramar P, Delemotte L, Lebar A, Kotulska M, Tarek M, Miklavcic D (2012) Molecular-level characterization of lipid membrane electroporation using linearly rising current. J Membr Biol 245:651

Lantzsch G, Binder H, Heerklotz H (1994) Surface area per molecule in lipid/c12en. Membranes as seen by fluorescence resonance energy transfer. J Fluoresc 4:339

Levine ZA, Vernier PT (2010) Life cycle of an electropore: field-dependent and field-independent steps in pore creation and annihilation. J Membr Biol 236:27–36

Marty M, Sersa G, Garbay J, Gehl J, Collins C et al (2006) Electrochemotherapy—an easy, highly effective and safe treatment of cutaneous and subcutaneous metastases: results of ESOPE (European Standard Operating Procedures of Electrochemotherapy) study. Eur J Cancer Suppl 4:3

Mir LM, Orlowski S, Belehradek J, Teissie J, Rols M, Sersa G, Miklavcic D, Gilbert R, Heller R (1995) Biomedical application of electric pulses with special emphasis on antitumor electrochemotherapy. Bioelectrochem Bioenerg 38:203–207

Mir LM, Glass LF, Serša G, Teissié J, Domenge C, Miklavčič D, Jaroszeski MJ, Orlowski S, Reintgen DS, Rudolf Z, Belehradek M, Gilbert R, Rols MP, Belehradek JJ, Bachaud JM, DeConti R, Štabuc B, Čemažar M, Coninx P, Heller R (1998) Effective treatment of cutaneous and subcutaneous malignant tumours by electrochemotherapy. Br J Cancer 77:2336–2342

Mir LM, Bureau MF, Gehl J, Rangara R, Rouy D, Caillaud JM, Delaere P, Branellec D, Schwartz B, Scherman D (1999) High-efficiency gene transfer into skeletal muscle mediated by electric pulses. Proc Natl Acad Sci USA 96:4262–4267

Miyamoto S, Kollman PA (1992) Settle—an analytical version of the shake and rattle algorithm for rigid water models. J Comput Chem 13:952–962

Neu JC, Krassowska W (1999) Asymptotic model of electroporation. Phys Rev E 59:3471

Neumann E, Schaefer-Ridder M, Wang V, Hofschneider PN (1982) Gene transfer into mouse myeloma cells by electroporation in high electric fields. EMBO Eur Mol Biol Organ J 1:841

Neumann E, Kakorin S, Toensing K (1999) Fundamentals of electroporative delivery of drugs and genes. Bioelectrochem Bioenerg 48:3–16

Nuccitelli R, Pliquett U, Chen X, Ford W, James Swanson R, Beebe SJ, Kolb JF, Schoenbach KH (2006) Nanosecond pulsed electric fields cause melanomas to self-destruct. Biochem Biophys Res Commun 343:351

Pakhomov AG, Kolb JF, White JA, Joshi RP, Xiao S, Schoenbach KH (2007) Long-lasting plasma membrane permeabilization in mammalian cells by nanosecond pulsed electric field (nspef). Bioelectromagnetics 28:655

Panje WR, Hier MP, Garman GR, Harrell E, Goldman A, Bloch I (1998) Electroporation therapy of head and neck cancer. Ann Otol Rhinol Laryngol 107:779

Pastushenko VF, Chizmadzhev YA, Arakelyan VB (1979) Electric breakdown of bilayer lipid membranes: II. Calculations of the membrane lifetime in the steady-state diffusion approximation. Bioelectrochem Bioenerg 6:53

Pathria RK (1972) Statistical mechanics. Pergamon, Oxford

Potter H (1988) Electroporation in biology: methods, applications and instrumentation. Anal Biochem 174:361

Rabussay D, Widera G (2002) Drug development and delivery including speciality pharma. Electroporation Ther 2:1

Siu SW, Vácha R, Jungwirth P, Böckmann RA (2008) Biomolecular simulations of membranes: physical properties from different force fields. J Chem Phys 128(125):103

Smithies O, Gregg RG, Boggs SS, Koralewski MA, Kucherlapati RS (1985) Insertion of DNA sequences into the human chromosomal fl-globin locus by homologous recombination. Nature 317:233

Snoj M, Cemazar M, Srnovrsink T, Kosir SP, Sersa G (2009) Limb sparing treatment of bleeding melanoma recurrence by electrochemotherapy. Tumori 95:398

Sugar IP (1979) A theory of the electric field-induced phase transition of phospholipid bilayers. Biochem Biophys Res Commun 556:72

Sun S, Wong JTY, Zhang TY (2011) Atomistic simulations of electroporation in water preembedded membranes. J Phys Chem B 115:13355–13359

Suzuki T, Shin B, Fujikura K, Matsuzaki T, Takata K (1998) Direct gene transfer into rat liver cells by in vivo electroporation. FEBS Lett 425:436–440

Tarek M (2005) Membrane electroporation: a molecular dynamics simulation. Biophys J 88:4045

Tekle E, Astumian RD, Chock PB (1994) Selective and asymmetric molecular transport across electroporated cell membranes. Proc Natl Acad Sci USA 91:11512

Tekle E, Astumian RD, Friauf WA, Chock PB (2001) Asymmetric pore distribution and loss of membrane lipid in electroporated dopc vesicles. Biophys J 81:960

Tieleman D, Leontiadou H, Mark A, Marrink S (2003) Simulation of pore formation in lipid bilayers by mechanical stress and electric fields. J Am Chem Soc 125:6382

van der Spoel D, Lindahl E, Hess B, van Buuren AR, Apol E, Meulenhoff PJ, Tieleman DP, Sijbers ALTM, Feenstra KA, van Drunen R, Berendsen HJC (2010) Gromacs user manual, version 4.5.4. www.gromacs.org

Vernier PT, Sun Y, Marcu L, Craft CM, Gundersen MA (2004) Nanoelectropulse-induced phosphatidylserine translocation. Biophys J 86:4040

Vernier PT, Levine ZA, Wu YH, Joubert V, Ziegler MJ, Mir LM, Tieleman DP (2009) Electroporating fields target oxidatively damaged areas in the cell membrane. PLoS One 4:e7966

Weaver J (2000) Electroporation of cells and tissues. IEEE Trans Plasma Sci 28:24–33

Weaver JC, Mintzer RA (1981) Decreased bilayer stability due to transmembrane potentials. Phys Lett 86A:57–59

Wong TK, Neumann E (1982) Electric field-induced gene transfer. Biochem Biophys Res Commun 107:584

Yang NS (1985) Transient gene expression in electroporated plant cells. Trends Biotechnol 3:191

Zimmermann U, Vienken J (1982) Electric field-induced cell to cell fusion. J Membr Biol 67:165

Zimmermann U, Vienken J, Pilwat G (1980) Development of drug carrier systems: electric field induced effects in cell membranes. J Electroanal Chem 116:553